JOURNAL OF MATERIALS SCIENCE **34** (1999) 5803–5809

Sintering and crystallization of $(SrO{\cdot}SiO_2)$-$(SrO{\cdot}Al_2O_3{\cdot}2SiO_2)$ glass-ceramics

YUN-MO SUNG*
Department of Materials Science & Engineering, Daejin University, Pocheon-koon, Kyunggi-do 487-711, South Korea
E-mail: ymsung@road.daejin.ac.kr

JOON SIK PARK
Department of Materials Science & Engineering, University of Wisconsin-Madison, Madison, Wisconsin 53706, USA

In the ternary SrO-Al_2O_3-SiO_2 system the pseudobinary join composition of 50 wt % $SrO{\cdot}SiO_2$–50 wt % $SrO{\cdot}Al_2O_3{\cdot}2SiO_2$ (SS-SA2S) showed a glass melting temperature of ~1500 °C and a crystallization peak temperature of ~1100 °C. The (SS-SA2S) glass-ceramic pellets prepared by cold pressing and pressureless sintering, showed very low porosity. The (SS-SA2S) glass-ceramics containing B_2O_3 and those containing B_2O_3 and TiO_2 revealed crystallization peak temperatures of ~1000 °C and unexpectedly high porosity. By applying Kissinger analyses to the DTA data the activation energy values for crystallization of the three glass-ceramics were determined to range from 196 to 255 kJ/mol. The Ozawa analyses on the DTA data gave the Avrami parameter values at 3.69 to 3.95. The X-ray diffraction (XRD) patterns from the three glass-ceramics revealed formation of the equilibrium crystalline phases of $SrO{\cdot}SiO_2$ and $SrO{\cdot}Al_2O_3{\cdot}2SiO_2$ (monocelsian). © *1999 Kluwer Academic Publishers*

1. Introduction

Due to unique properties such as high strength, low density, chemical stability, low thermal expansion and low dielectric properties, glass-ceramics have been used for various purposes including high-temperature structural applications and electronic packaging [1]. The sintering of glass powders followed by crystallization of the glass body can give huge benefit to the glass-ceramic fabrication since this method can reduce processing temperature and make the fabrication of complex-shape components possible using variety of conventional ceramic-forming techniques [2–8].

Strontium aluminosilicate composition of $SrO{\cdot}Al_2O_3{\cdot}2SiO_2$ (SA2S) forming monoclinic celsian as a primary crystalline phase, has been studied mainly for the use as matrix materials for high-temperature ceramic composites [9, 10]. The major reasons of this include its high melting point of ~1700 °C, low thermal expansion coefficient of $\sim 2.5 \times 10^{-6}$/°C, oxidation resistance and phase stability up to the melting point [11–13].

Bansal and Hyatt [11] fabricated stoichiometric (Sr, Ba)$O{\cdot}Al_2O_3{\cdot}2SiO_2$ glass-ceramics by sintering and hot isostatic pressing (HIP). The SA2S glass-ceramic samples which were cold isostatic pressed and sintered, showed density values ranging from 66 to 98% of the theoretical value depending upon the final sintering schedule. The SA2S glass-ceramic samples processed at 900 °C showed formation of both the hexacelsian and monocelsian phases, while those processed at 1100 °C showed only monocelsian phase. They [13] also studied the crystallization kinetics of the stoichiometric SA2S glass and obtained the crystal growth activation energy of 534 kJ/mol and Avrami parameter of 4.2. By using XRD technique they found that the phase transformation of hexacelsian to monocelsian in the SA2S system occurred after 1 h at 1100 °C. However, in order to obtain a homogeneous SA2S glass melt they raised the furnace temperature to 2000 °C which is a too high temperature for ceramic industries to obtain for the fabrication of wide range of glass-ceramics.

Sung [7, 8] prepared off-stoichiometric cordierite ($2MgO{\cdot}2Al_2O_3{\cdot}5SiO_2$) glass-ceramics with additives of B_2O_3, P_2O_5 and/or TiO_2 and found that they have high sintering ability and good mechanical properties. The off-stoichiometric cordierite glass-ceramics with additives, also showed much reduced processing temperatures such as glass melting and crystallization peak temperatures.

The focus of this study was on the development of the glass-ceramics which have lowered glass melting and crystallization peak temperatures, while maintaining high sintering ability. The glass-ceramics with off-stoichiometric binary join composition of 50 wt % ($SrO{\cdot}SiO_2$)–50 wt % ($SrO{\cdot}Al_2O_3{\cdot}2SiO_2$) (SS-SA2S), were produced by cold pressing of the glass

* Author to whom all correspondence should be addressed.

powders and sintering followed by crystallization heat treatments. Their sintering and crystallization behaviors were compared with those of the stoichiometric SA2S glass-ceramics studied by previous researchers. Also, the effect of sintering aid (B_2O_3) and nucleation agent (TiO_2) on the sintering and crystallization behaviors of the off-stoichiometric (SS-SA2S) glass-ceramics was studied in detail.

2. Experimental

High purity powders of $SrCO_3$, Al_2O_3, SiO_2, B_2O_3 and TiO_2 from Aldrich Chemical (Milwaukee, WI, USA) were used for starting materials. Table I lists the composition of each glass prepared for present study. The (SS-SAS) composition indicating 50 wt % $SrO{\cdot}SiO_2$–50 wt % $SrO{\cdot}Al_2O_3{\cdot}2SiO_2$ corresponds to 47.55 wt % SrO, 15.65 wt % Al_2O_3 and 36.80 wt % SiO_2. Fig. 1 shows the equilibrium phase diagram of $SrO\text{-}Al_2O_3\text{-}SiO_2$ system [14]. For this system the liquidus projection was not available and only the alkemade lines were presented on the phase diagram. The "*x*" denotes the composition of (SS-SA2S). The powders were well mixed using a zirconia-ball milling. The powder mixtures were loaded inside a platinum crucible and brought to a resistance furnace with super kanthal heating elements for glass melting. The weight of target glass was 40 g. The powder mixture was heated to 1000 °C for 1 h for calcination and further heated to 1600 °C for 1 h for complete glass melting. The platinum crucible containing the glass melt was quenched into distilled water and clear glass fragments were obtained. The glass fragments were dried and hand ground using a high-purity alumina motar and pestle. The hand-ground glass powders were zirconia-ball milled to the average particle size of 3–5 μm. Each of the glass powders was analyzed for various temperatures such as glass transition (T_g), crystallization onset (T_o) and crystallization peak (T_p) using differential thermal analyses (DTA: SETARAM TGDTA-92, France). The DTA results were further analyzed for the activation energy for crystallization and crystallization mode using Kissinger and Ozawa analyses, respectively. These fine glass powders were pelletized using a steel die and hydraulic press under 3000 psi at a room temperature. The glass pellets were 4 mm in diameter and 2 mm in thickness. The cold-pressed pellets loaded inside a platinum boat were brought to the furnace for sintering at 900 °C which is a temperature between the T_g and T_o. The sintered glass pellets were further heated for crystallization at 1100 °C which is almost T_p. The duration at each of the sintering and crystallization temperatures was 2 and 4 h, respectively. The glass-ceramic pellets were analyzed for density using the Archimedes principle. The glass-ceramic pellets were cut in the middle by using a low-speed diamond saw and mounted in epoxy resin. The cross sections of the glass-ceramic pellets were polished using SiC papers (grit # 600 and 1000) and alumina powders (1.0 and 0.5 μm). The polished samples were coated by a gold sputtering. The scanning electron microscopy (SEM: JSM-6100, Jeol, Japan) was performed on the polished and gold-coated samples to examine the microstructure of the glass-ceramics. The X-ray diffraction (XRD: Nicolet Stoe Transmission/Bragg-Brentano, Stoe Co., Germany) was also performed on the powdered glass-ceramics with a CuK_α source, a 5-s time constant, a 10–60° scan, and 0.05° step size. The phase identification was done by the comparison of the peak locations and intensities with the data listed in JCPDS cards (#38-1454 for $SrO{\cdot}Al_2O_3{\cdot}2SiO_2$, #34-99 for $SrO{\cdot}SiO_2$).

TABLE I Composition of the glasses prepared for present study

	Elements (wt %)				
Glasses	SrO	Al_2O_3	SiO_2	B_2O_3	TiO_2
(SS-SA2S)	47.55	15.65	36.80	—	—
(SS-SA2S)B	46.12	15.18	35.70	3.00	—
(SS-SA2S)BT	44.70	14.71	34.59	3.00	3.00

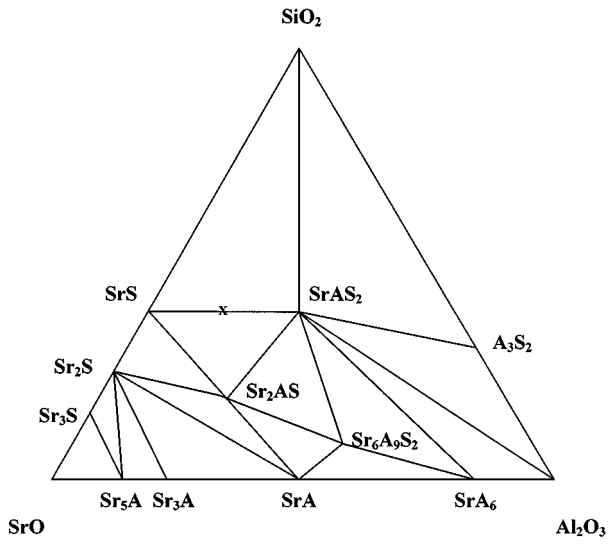

Figure 1 The equilibrium phase diagram of $SrO\text{-}Al_2O_3\text{-}SiO_2$ system showing only the alkemade triangles [14].

3. Results

The (SS-SA2S), (SS-SA2S)B and (SS-SA2S)BT compositions were completely melted to form homogeneous glass melts at 1600 °C. The (SS-SA2S)BT glass showed very light yellowish color. By using the XRD analyses the non-crystallinity was identified from the three glasses. The glass transition and crystallization trends of the glasses were investigated using DTA. DTA scan curves from the three glasses at the heating rates of 10, 15, 20, 30 and 40 °C/min are shown in Figs 2–4. In order to show the difference in the glass transition and crystallization DTA scan curves of the three glasses with a heating rate of 20 °C/min are shown and compared in Fig. 5. Table II lists the T_g and T_p values of the stoichiometric SA2S glass and the three non-stoichiometric (SS-SA2S), (SS-SA2S)B and (SS-SAS)BT glasses at a heating rate of 20 °C/min. The temperature values for the stoichiometric SA2S glass were taken from Hyatt and Bansal's data [13]. The off-stoichiometric (SS-SA2S) glass shows T_p value 63 °C higher than that of the stoichiometric SA2S glass. The other off-stoichiometric glasses, (SS-SA2S)B and (SS-SAS)BT show the T_p values which were approximately 100 °C lower than that of

TABLE II Summary of glass transition (T_g) and crystallization peak (T_p) temperatures of the glass powders prepared for present study

	Glass transition temp. (°C)					Crystallization peak temp. (°C)				
	DTA scan rates (°C/min)					DTA scan rates (°C/min)				
Glasses	10	15	20	30	40	10	15	20	30	40
SA2S[a]	880	—	884	892	895	1032	—	1053	1064	1075
(SS-SA2S)	774	782	786	791	798	1077	1104	1116	1131	1160
(SS-SA2S)B	717	725	729	741	751	970	991	1013	1021	1059
(SS-SA2S)BT	718	718	725	734	740	985	1007	1019	1040	1065

[a]The T_g and T_p values of the SA2S glass are from Hyatt and Bansal's DSC data [13].

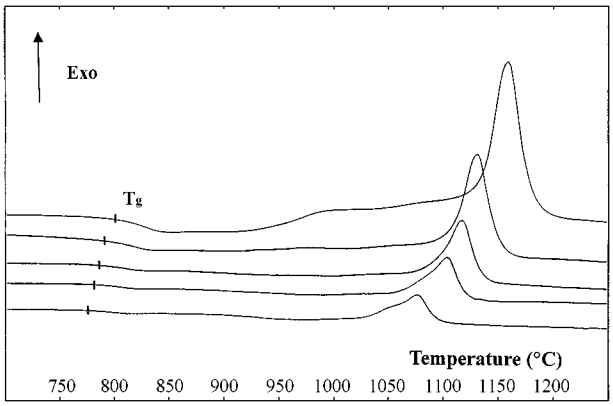

Figure 2 The differential thermal analysis (DTA) scan curves of (SS-SA2S) glass. Each of the scan curves corresponds to the scan rates of 10, 15, 20, 30 and 40 °C/min, respectively from the bottom to the top.

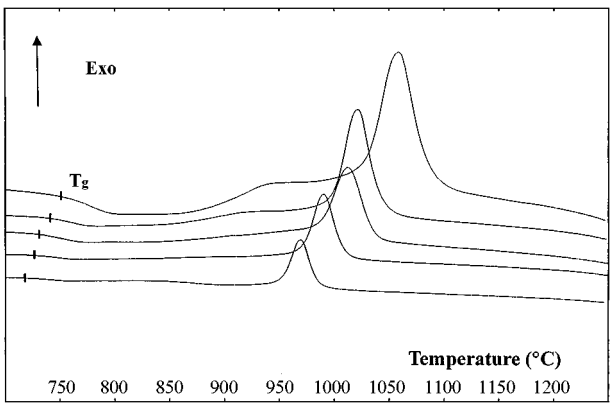

Figure 3 The differential thermal analysis (DTA) scan curves of (SS-SA2S)B glass. Each of the scan curves corresponds to the scan rates of 10, 15, 20, 30 and 40 °C/min, respectively from the bottom to the top.

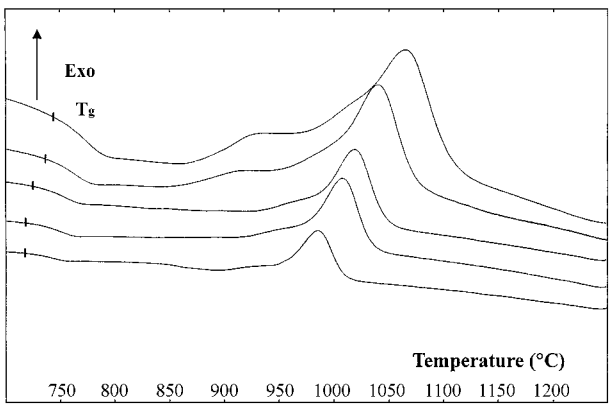

Figure 4 The differential thermal analysis (DTA) scan curves of (SS-SA2S)BT glass. Each of the scan curves corresponds to the scan rates of 10, 15, 20, 30 and 40 °C/min, respectively from the bottom to the top.

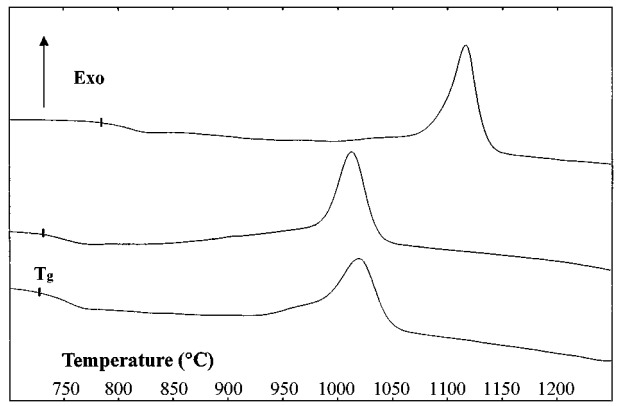

Figure 5 The comparison of the DTA scan curves of (a) (SS-SA2S), (b) (SS-SA2S)B and (c) (SS-SA2S)BT glasses at a scan rate of 20 °C/min.

the (SS-SA2S) glass. Unexpectedly, the (SS-SA2S)B and (SS-SA2S)BT glasses show very close T_p values.

For the DTA scan curves the faster the heating rates, the higher the peak temperatures and the larger the peak heights become. The variation of the crystallization peaks depending upon the DTA scan rates can be used to estimate the activation energy for crystallization and crystallization mode. The activation energy values for the crystallization of the glasses can be estimated by using following Kissinger analysis [15].

$$\ln\left(\frac{\phi}{T_p^2}\right) = -\frac{E_{ck}}{RT_p} + \text{const.} \qquad (1)$$

where ϕ is the DTA scan rate (°C/min), T_p is the crystallization peak temperature (°K), E_{ck} is the activation energy (kJ/mol) for the crystallization from Kissinger equation and R is the gas constant (8.3144 J/mol°K). From the Equation 1 the Kissinger plot of $\ln(\phi/T_p^2)$ vs $1000/T_p$ can be produced by substituting each DTA scan rate (ϕ) and its corresponding T_p value. Fig. 6 shows the Kissinger plots of (SS-SA2S), (SS-SA2S)B and (SS-SA2S)BT glasses. The activation energy for crystallization (E_{ck}) can be determined from the slope ($-E_{ck}/R$) of each Kissinger plot. The activation energy values of (SS-SA2S), (SS-SA2S)B and (SS-SA2S)BT glasses, were determined to be 255, 196 and 222 kJ/mol, respectively.

The crystallization mode of the glasses can be identified by using following Ozawa analysis [16].

$$\{\ln[-\ln(1-x)]\}_T = -n\ln\phi + \text{const.} \qquad (2)$$

where x is the volume fraction crystallized at a fixed temperature T when heated at ϕ that is, the ratio of the

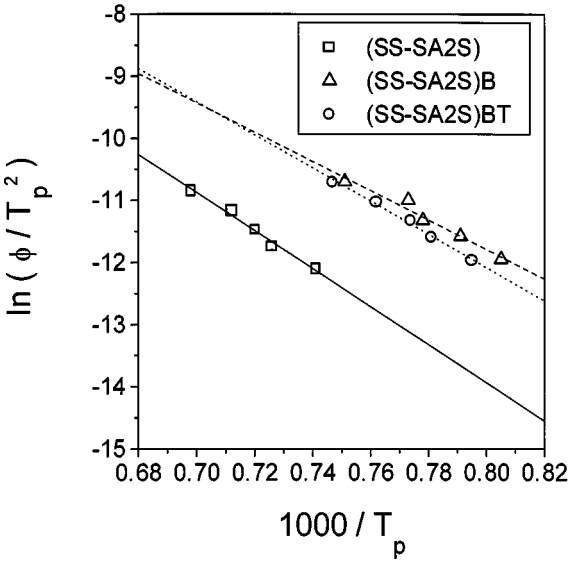

Figure 6 The Kissinger plots of (SS-SA2S), (SS-SA2S)B and (SS-SA2S)BT glasses. From the slopes of the lines the activation energy values for the crystallization were determined as 255, 196 and 222 kJ/mol, respectively.

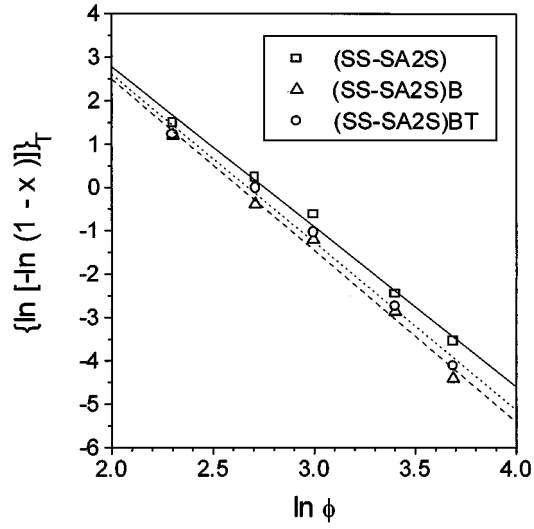

Figure 7 The Ozawa plots of (SS-SA2S), (SS-SA2S)B and (SS-SA2S)BT glasses. From the slopes of the lines the Avrami parameter values were determined to be 3.69, 3.95 and 3.87, respectively.

partial area at T to the total area of the crystallization exotherm. The n is the Avrami parameter which indicating a crystallization mode. The fixed temperature, T was 1110, 990 and 1010 °C for the (SS-SA2S)B, (SS-SA2S)B and (SS-SA2S)BT glasses, respectively. When surface crystallization dominates, $n \sim 1$, and when bulk crystallization dominates, $n \geq 3$. When both the surface and bulk crystallization occur n has a value between 1 and 3. By substituting ϕ values and corresponding x values into the Equation 2 the Ozawa plots of the three glasses were created in Fig. 7. From the slopes of the Ozawa plots the Avrami parameter values of the (SS-SA2S), (SS-SA2S)B and (SS-SA2S)BT glasses were determined as 3.69, 3.95 and 3.87, respectively. The DTA results were summarized in Table III.

The glass-ceramic pellets sintered at 900 °C for 2 h and crystallized at 1100 °C for 4 h, were analyzed for density using the Archimedes method. The density

TABLE III Summary of DTA results of the glass powders prepared for present study

Glasses	Activation energy for crystallization, E_{ck} (kJ/mol)	Avrami parameter, n
SA2S[a]	534	4.2 ± 0.4
(SS-SA2S)	255	3.69
(SS-SA2S)B	196	3.95
(SS-SA2S)BT	222	3.87

[a]The activation energy for crystallization and Avrami parameter of SA2S glass powder are from Hyatt and Bansal's result [13].

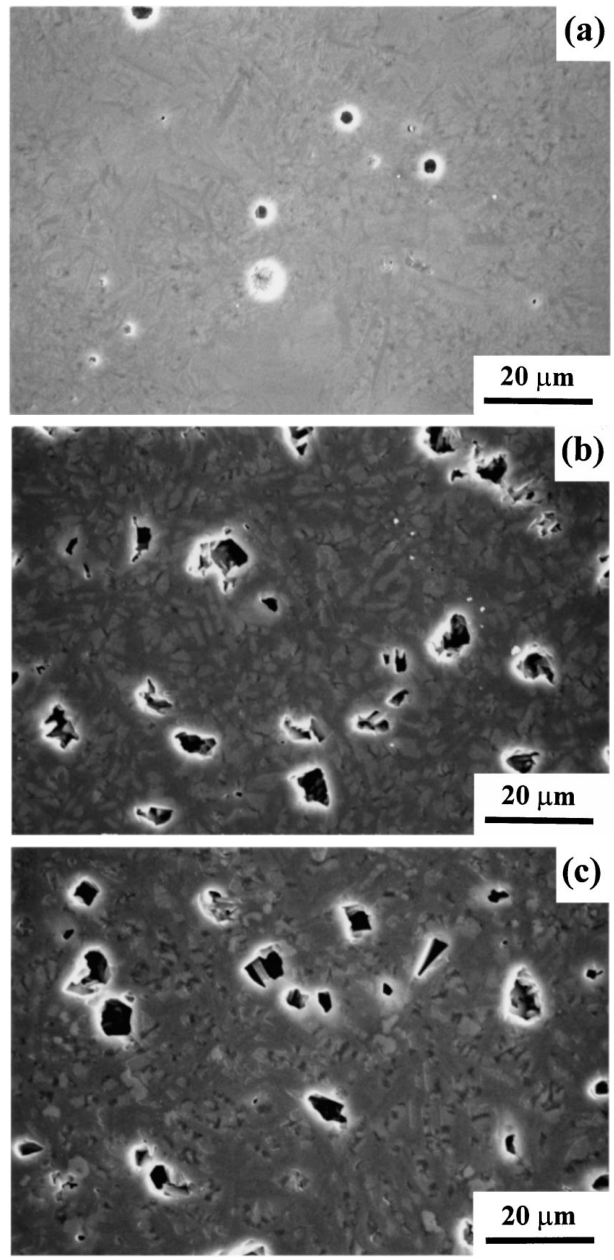

Figure 8 The scanning electron micrographs (SEM) of (a) (SS-SA2S), (b) (SS-SA2S)B and (c) (SS-SA2S)BT glass-ceramics.

value of (SS-SA2S) glass-ceramic pellets was determined as 3.33 while those of (SS-SA2S)B and (SS-SA2S)BT glass-ceramic pellets were determined to be 3.15 and 3.12 g/cm^3, respectively.

The scanning electron micrographs (SEM) on the glass-ceramics were shown in Fig. 8a, b and c. The microstructure of the (SS-SA2S) glass-ceramic showed

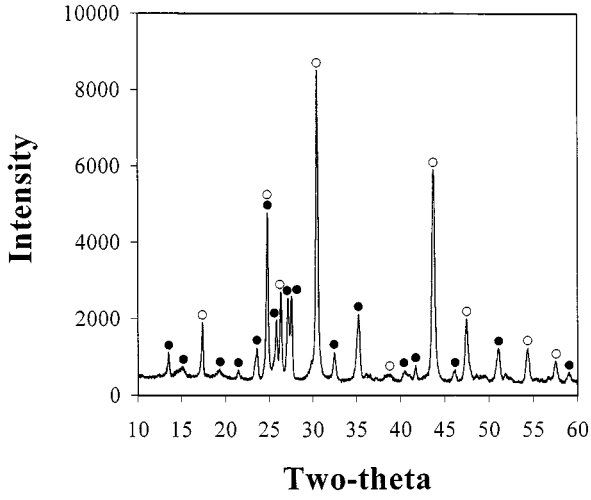

Figure 9 The X-ray diffraction (XRD) patterns of the (SS-SA2S) glass-ceramic showing formation of the equilibrium phases of $SrO{\cdot}SiO_2$ (○) and $SrO{\cdot}Al_2O_3{\cdot}2SiO_2$ (●). The other (SS-SA2S)B and (SS-SA2S)BT glass-ceramics showed almost identical XRD patterns.

low porosity while those of the (SS-SA2S)B and (SS-SA2S)BT glass-ceramics showed relatively high porosity. This microstructural analysis well corresponds to the density measurements.

The X-ray diffraction (XRD) patterns from the (SS-SAS), (SS-SAS)B and (SS-SAS)BT glass-ceramics sintered at 900 °C and crystallized at 1100 °C were almost identical and showed formation of the crystalline phases of $SrO{\cdot}SiO_2$ and $SrO{\cdot}Al_2O_3{\cdot}2SiO_2$. Fig. 9 shows the XRD pattern from the powdered (SS-SA2S) glass-ceramic which representing the XRD patterns of all the three glass-ceramics. No trend of non-crystallinity was found from the diffraction patterns and the peak intensities from the $SrO{\cdot}SiO_2$ phase were higher than those from the $SrO{\cdot}Al_2O_3{\cdot}2SiO_2$ phase.

4. Discussion

The practical melting temperature to obtain the homogeneous (SS-SA2S) glass melts was around 1600 °C which is much lower than the practical melting temperature (∼1800 °C) of the stoichiometric SA2S celsian composition. Due to this lowered melting temperature one can fabricate a glass-ceramic readily with less energy cost.

The glass transition and crystallization behaviors of a glass can give the key information to the glass-ceramic fabrication. According to the Hyatt and Bansal's DSC data [13] the glass transition temperature (T_g) of the stoichiometric SA2S celsian with a scan rate of 20 °C/min, was 884 °C while those of the glasses prepared for present study, (SS-SA2S), (SS-SA2S)B and (SS-SA2S)BT, were 774, 717 and 718 °C, respectively. The lowered glass transition implies reduced viscosity of a glass. The effect of a sintering aid of B_2O_3 is very clear since the (SS-SA2S)B and (SS-SA2S)BT glasses show the T_g lowered by 60 °C compared to the (SS-SA2S) glass. The addition of B_2O_3 could reduce the strong connectivity of the three-dimensional chain structure of a silicate glass thus, can lower its glass viscosity.

The crystallization peak temperature (T_p) of the stoichiometric SA2S glass with a scan rate of 20 °C/min was 1053 °C while those of the (SS-SA2S), (SS-SA2S)B and (SS-SA2S)BT glasses were 1116, 1013 and 1019 °C, respectively. The crystallization of a glass can take place by rearrangement of ions randomly oriented in it thus, diffusion process is involved. Since the (SS-SA2S)B and (SS-SA2S)BT glasses have low viscosity they can readily crystallize and thus, have lower crystallization peak temperatures (T_p's) compared to the (SS-SA2S) glass. The addition of nucleation agent, TiO_2, seems not to be effective since the T_p's of the (SS-SA2S)B and (SS-SA2S)BT glasses show very close values.

A careful look at the DTA scan curve of a glass with a high DTA scan rate of 30 or 40 °C/min reveals that there is a secondary peak near 900–1000 °C. For the DTA scan of 40 °C/min the (SS-SA2S), (SS-SA2S)B and (SS-SA2S)BT glasses showed secondary crystallization peak temperatures of 993, 943 and 929 °C, respectively. Also, the crystallization onset temperatures (T_o) of the glass-ceramics were 939, 876 and 867 °C, respectively. By XRD analyses on the samples quenched right after heated up to the secondary peak temperatures it was found that the secondary peaks correspond to the crystallization of a part of the glass to the $SrO{\cdot}SiO_2$ phase. The incorporation of nucleation agent, TiO_2 into the glass may have enhanced the crystallization of the $SrO{\cdot}SiO_2$ phase by forming titanates such as $Al_2Ti_2O_7$. The fact that the addition of few percentage of TiO_2 into an alkali-aluminosilicate glass forms titanates such as $Al_2Ti_2O_7$, has been reported by Barry *et al*. [17], Doherty *et al*. [18] and Hsu and Speyer [19]. The light yellowish color in a glass has commonly been found in the Li_2O-Al_2O_3-SiO_2 and MgO-Al_2O_3-SiO_2 glasses containing few percentage of TiO_2. Also, as for the present glasses only the (SS-SA2S)BT glass showed this color and the other (SS-SA2S) and (SS-SA2S)B glasses did not. This difference supports that titanates formed in the asquenched (SS-SA2S)BT glass. However, the exact nature of the titanates formed in the (SS-SA2S)BT glass is not clear at this stage. The primary peaks, thus represent the crystallization of the rest portion of the glass to the $SrO{\cdot}Al_2O_3{\cdot}2SiO_2$ phase. The $SrO{\cdot}Al_2O_3{\cdot}2SiO_2$ phase thus, can nucleate and grow around the $SrO{\cdot}SiO_2$ crystals. Therefore, the formation of $SrO{\cdot}Al_2O_3{\cdot}2SiO_2$ phase would not be affected by the addition of TiO_2. Thus, the (SS-SA2S)B and (SS-SA2S)BT glasses have very close T_p values. The lowered viscosity by addition of B_2O_3 seems to play a major role in decreasing the T_p values of the (SS-SA2S)B and (SS-SA2S)BT glasses.

The activation energy values for crystallization of the $SrO{\cdot}Al_2O_3{\cdot}2SiO_2$ phase obtained by using the Kissinger method indicate that the present glasses have much lower values (255, 196 and 222 kJ/mol) than that (534 kJ/mol) of the stoichiometric SA2S glass [13]. This difference would occur since for the (SS-SA2S), (SS-SA2S)B and (SS-SA2S)BT glasses the pre-existing $SrO{\cdot}SiO_2$ crystals can act as

heterogeneous nucleation sites for the formation of the $SrO{\cdot}Al_2O_3{\cdot}2SiO_2$ phase. The reason that the (SS-SA2S)B and (SS-SA2S)BT glasses have lower activation energy values than the (SS-SA2S) glass would be explained by the low viscosity of the glass remained after forming the $SrO{\cdot}SiO_2$ crystals. This low viscosity of the remaining glass also would come from the B_2O_3 addition.

The crystallization mode of a glass has a practical importance in the usage of it and also in the fabrication of a glass-ceramic since the surface crystallization mode may introduce large thermal expansion difference at the boundary between the glass phase and crystallized phase, building up high tensile stress [20]. This high tensile stress at the interface may cause total failure of the glass. On the other hand, in the case of the bulk crystallization mode where the crystal growth occurs at the finely distributed precursor nuclei in the glass, the huge thermal expansion coefficient gradient across the whole glass body does not occur, and the glass body is safe against the thermal failure. Thus, from this perspective the bulk crystallization is desirable compared to the surface crystallization. The crystallization mode of a glass can be determined by the Avrami parameter value (n). As expected from the DTA and XRD data all of the (SS-SA2S), (SS-SA2S)B and (SS-SA2S)BT glasses showed high Avrami parameters of 3.69–3.95 which represent high bulk crystallization tendency of them. Due to the $SrO{\cdot}SiO_2$ crystals distributed in a glass body, acting as nucleation sites the $SrO{\cdot}Al_2O_3{\cdot}2SiO_2$ phase formation would be a strong bulk crystallization process.

The density value of the (SS-SA2S) glass-ceramic was high while those of the (SS-SA2S)B and (SS-SA2S)BT glass-ceramics were low. The sintering ability of a glass can be estimated from the temperature range between crystallization onset and glass transition, (T_o–T_g). The viscosity of a glass rapidly decreases when it is heated above T_g at which the glass chain structure is broken but dramatically increases when crystallization initiates. Thus, the sintering of a glass occurs at the temperature range of T_o–T_g. If the temperature range is small premature crystallization can occur before the completion of the sintering. Once the premature crystallization occurs the viscosity of a glass increases markedly and the sintering ends. Thus, high sintering ability cannot be expected from a glass with small temperature range of T_o–T_g. For the (SS-SA2S), (SS-SA2S)B and (SS-SA2S)BT glasses the T_o corresponds to the crystallization onset temperature of the $SrO{\cdot}SiO_2$ phase. The T_o–T_g values of the glasses are 141, 125 and 127 °C, respectively. This result is in good agreement with the density data.

The theoretical density value of the glass-ceramics can be determined by using each theoretical density value of the $SrO{\cdot}SiO_2$ (3.660 g/cm^3) and $SrO{\cdot}Al_2O_3{\cdot}2SiO_2$ (monocelsian; 3.084 g/cm^3) crystals and the mol % of each phase. The weight percentage (50 wt % $SrO{\cdot}SiO_2$–50 wt % $SrO{\cdot}Al_2O_3{\cdot}2SiO_2$) of the glass-ceramics can be converted to the molar percentage (66.55 mol % $SrO{\cdot}SiO_2$–33.46 mol % $SrO{\cdot}Al_2O_3{\cdot}2SiO_2$). The theoretical density of the (SS-SA2S) glass-ceramic thus, is determined as 3.467 g/cm^3. Therefore, the (SS-SA2S), (SS-SA2S)B and (SS-SA2S)BT glass-ceramic pellets show 96, 91 and 90% of its theoretical density. In considering the fact that these glass-ceramics were fabricated using only pressureless sintering after cold pressing, the sintering ability of the (SS-SA2S) glass-ceramic is relatively high.

The SEM micrographs on the glass-ceramics well support the density measurements and DTA results. The (SS-SA2S)B and (SS-SA2S)BT glass-ceramics showed relatively high porosity compared to the (SS-SA2S) glass-ceramic. The contrasted texture in the micrographs comes from the compositional difference between the $SrO{\cdot}SiO_2$ and $SrO{\cdot}Al_2O_3{\cdot}2SiO_2$ phases. The former is brighter since it contains higher content of heavy strontium ions.

The XRD patterns on the glass-ceramics showed formation of the equilibrium phases of $SrO{\cdot}SiO_2$ and $SrO{\cdot}Al_2O_3{\cdot}2SiO_2$. No trend of non-crystallinity was found in the XRD patterns. As expected from the mol % value of each phase the peak intensity of the $SrO{\cdot}SiO_2$ phase was higher than that of the $SrO{\cdot}Al_2O_3{\cdot}2SiO_2$ phase. The $SrO{\cdot}Al_2O_3{\cdot}2SiO_2$ phase was identified to have a monocelsian structure. The precursor nuclei of $SrO{\cdot}SiO_2$ crystals must have enhanced the formation of monocelsian phase.

5. Conclusions

As an effort to develop a glass-ceramic material with low processing temperatures and high sintering ability the off-stoichiometric (SS-SA2S) compositions were studied for the sintering and crystallization behaviors. The (SS-SA2S) composition showed melting temperature ~100 °C lowered compared to the stoichiometric SA2S composition. Due to the reduced viscosity the (SS-SA2S)B and (SS-SA2S)BT glasses showed approximately 100 °C lowered crystallization peak temperature compared to the (SS-SA2S) glass. Also, most likely due to the pre-existing $SrO{\cdot}SiO_2$ crystals in a glass matrix the (SS-SA2S), (SS-SA2S)B and (SS-SA2S)BT glasses showed much lower activation energy values for crystallization than that of the stoichiometric SA2S glass. Avrami parameters of the three glasses showed very close values of 3.69–3.95, which indicating strong bulk crystallization tendency of them. The (SS-SA2S) glass has the biggest temperature range of T_o–T_g and thus, showed the highest density (96% of the theoretical density) among the three glasses. The SEM micrographs and XRD patterns reveal the formation of two equilibrium cystalline phases of $SrO{\cdot}SiO_2$ and $SrO{\cdot}Al_2O_3{\cdot}2SiO_2$.

In the light of the low processing temperature and high sintering ability the (SS-SA2S) glass-ceramics have high potential for variety of applications such as composite matrices, substrates for semiconductor packaging, heat exchanger parts, and so on. The mechanical properties of the (SS-SA2S) glass-ceramics will be reported later.

Acknowledgement

This study was supported by the Daejin University Research Grants in 1998. The authors would like to thank a reviewer for truly helpful comments and corrections.

References

1. G. H. BEALL and D. A. DUKE, in "Glass Science and Technology," Vol. 1, "Glass-Ceramic Technology," edited by D. R. Uhlmann and N. J. Kreidl (Academic Press, New York, 1983) p. 403.
2. E. M. RABINOVICH, in "Advances in Ceramics," Vol. 4, "Nucleation and Crystallization in Glasses," edited by J. H. Simmons, D. R. Uhlmann and G. H. Beall (American Ceramic Society, Columbus, OH, 1982) p. 327.
3. P. C. PANDA, W. M. MOBLEY and R. RAJ, *J. Amer. Ceram. Soc.* **72** (1989) 2361.
4. T. RUDOLPH, K.-L. WEISSKOPT, W. PANNHORST and G. PETZOW, *Glasstech. Ber.* **64** (1991) 305.
5. S. KNICKERBOCKER, M. R. TUZZOLO and S. LAWHORNE, *J. Amer. Ceram. Soc.* **72** (1989) 1873.
6. Y.-M. SUNG, S. A. DUNN and J. A. KOUTSKY, *J. Eur. Ceram. Soc.* **14** (1994) 455.
7. Y.-M. SUNG, *J. Mater. Sci.* **31** (1996) 5421.
8. *Idem., Ceram. Inter.* **23** (1997) 401.
9. N. P. BANSAL, *Mater. Sci. & Eng.* **A231** (1997) 117.
10. *Idem., J. Mater. Res.* **12** (1997) 745.
11. N. P. BANSAL, M. J. HYATT and C. H. DRUMMOND, III, *Ceram. Eng. Sci. Proc.* **12** (1991) 1222.
12. N. P. BANSAL and C. H. DRUMMOND, III, *J. Amer. Ceram. Soc.* **76** (1993) 1321.
13. M. J. HYATT and N. P. BANSAL, *J. Mater. Sci.* **31** (1996) 172.
14. P. S. DEAR, *Bull. Virginia Polytechnic Inst.* **50** (1957) 8.
15. H. E. KISSINGER, *J. Res. Natl. Bur. Stand. (US)* **57** (1956) 217.
16. T. OZAWA, *Polymer* **12** (1971) 150.
17. T. I. BARRY, D. CLINTON, L. A. LAY, R. A. MERCER and R. P. MILLER, *J. Mater. Sci.* **4** (1969) 596.
18. P. E. DOHERTY, D. W. LEE and R. S. DAVIS, *J. Amer. Ceram. Soc.* **55** (1970) 77.
19. J. HSU and R. F. SPEYER, *ibid.* **72** (1989) 2334.
20. Y.-M. SUNG and J.-H. SUNG, *J. Mater. Sci.* **33** (1998) 4733.

Received 30 September 1998
and accepted 23 June 1999